



# Identification of potential inhibitors of Zika virus targeting NS3 helicase using molecular dynamics simulations and DFT studies

Shashank Shekher Mishra<sup>1</sup> · Neeraj Kumar<sup>2</sup> · Bidhu Bhusan Karkara<sup>3</sup> · C. S. Sharma<sup>2</sup> · Sourav Kalra<sup>4</sup>

Received: 5 May 2022 / Accepted: 26 August 2022  
© The Author(s), under exclusive licence to Springer Nature Switzerland AG 2022

## Abstract

Despite the various research efforts towards the drug discovery program for Zika virus treatment, no antiviral drugs or vaccines have yet been discovered. The spread of the mosquito vector and ZIKV infection exposure is expected to accelerate globally due to continuing global travel. The NS3-Hel is a non-structural protein part and involved in different functions such as polyprotein processing, genome replication, etc. It makes an NS3-Hel protein an attractive target for designing novel drugs for ZIKV treatment. This investigation identifies the novel, potent ZIKV inhibitors by virtual screening and elucidates the binding pattern using molecular docking and molecular dynamics simulation studies. The molecular dynamics simulation results indicate dynamic stability between protein and ligand complexes, and the structures keep significantly unchanged at the binding site during the simulation period. All inhibitors found within the acceptable range having drug-likeness properties. The synthetic feasibility score suggests that all screened inhibitors can be easily synthesizable. Therefore, possible inhibitors obtained from this study can be considered a potential inhibitor for NS3 Hel, and further, it could be provided as a lead for drug development.

---

✉ Shashank Shekher Mishra  
shashankmedchem09@gmail.com

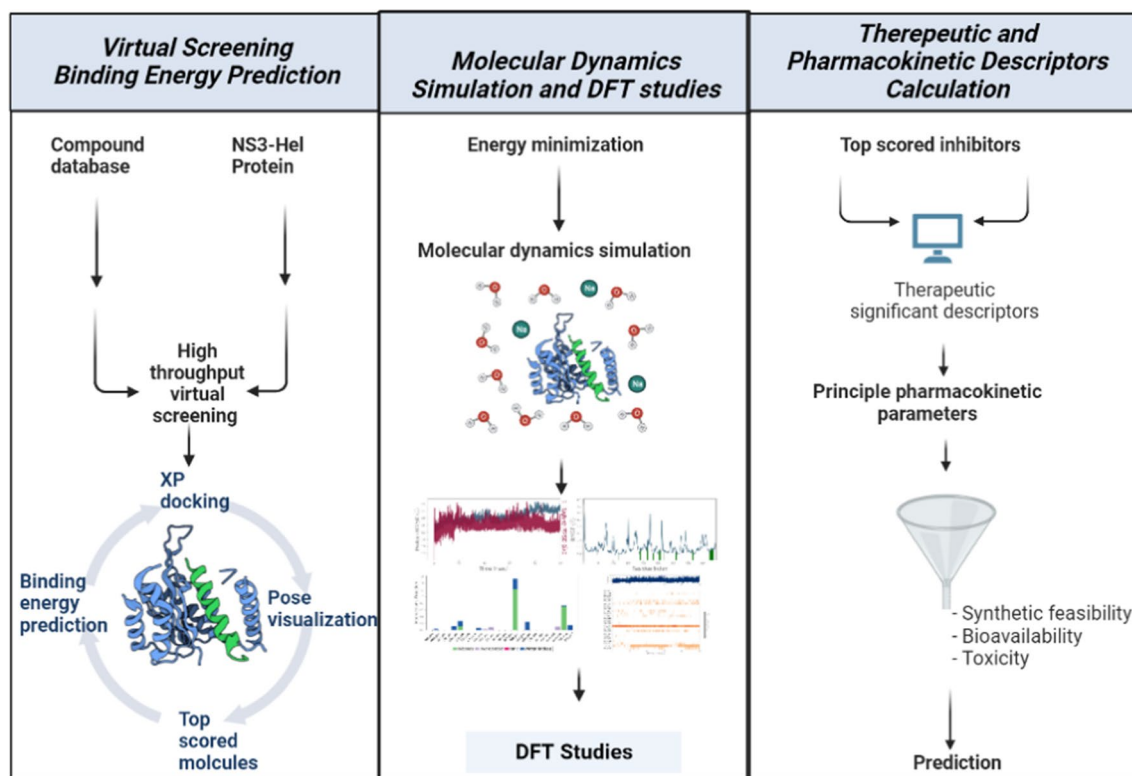
<sup>1</sup> Department of Pharmaceutical Chemistry, School of Pharmaceutical & Populations Health Informatics, DIT University, Dehradun 248009, India

<sup>2</sup> Department of Pharmaceutical Chemistry, Bhupal Nobles' College of Pharmacy, Bhupal Nobles' University, Udaipur 313001, India

<sup>3</sup> Department of Pharmaceutical Sciences, Vignan's Foundation for Science, Technology and Research, Vadlamudi, Guntur 522213, India

<sup>4</sup> National Institute of Pharmaceutical Education & Research, Mohali, Punjab, India

## Graphical abstract



**Keywords** Zika virus · Molecular dynamics simulations · Virtual screening · Synthetic feasibility · Toxicity · DFT

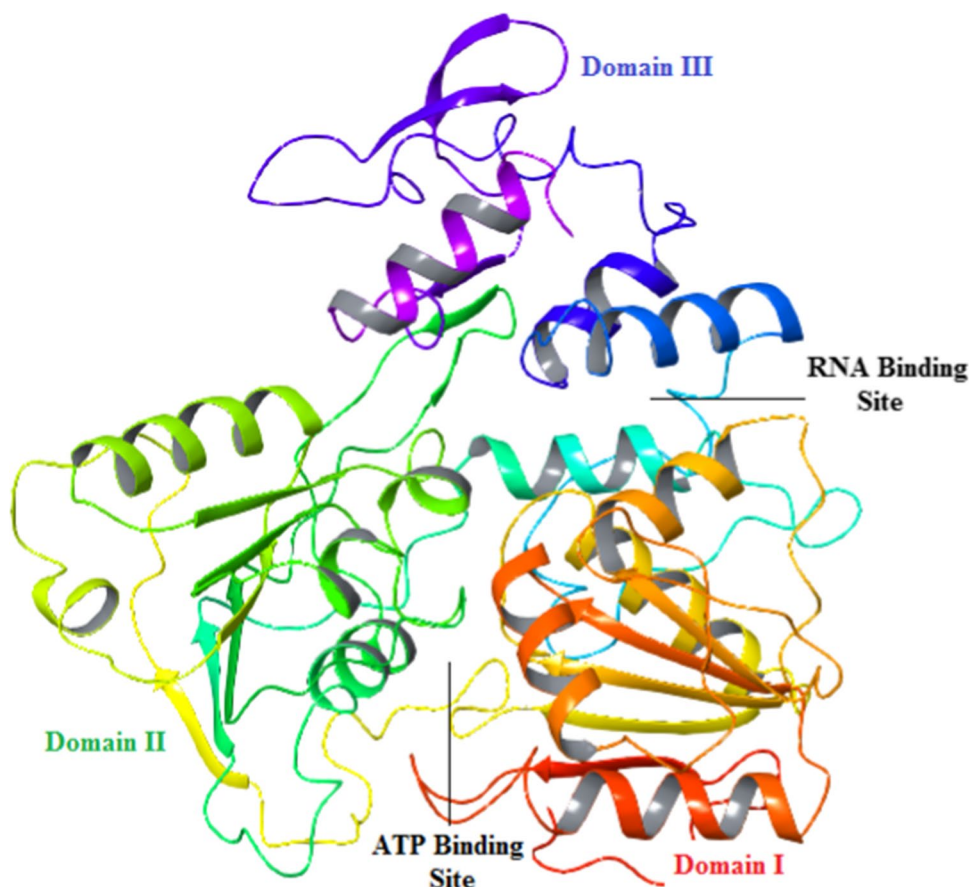
## Introduction

The Zika flavivirus (ZIKV) is an arthropod-borne virus and closely related to West Nile, Dengue, and Yellow Fever viruses [1]. ZIKV was first discovered in 1947 in the Zika forest of Uganda and isolated from multiple *Aedes* species, which serves as the primary epidemic vector and is also associated with ZIKV transmission to humans [2]. There were many cases of ZIKV reported in countries such as Tanzania, Uganda, Gabon, Egypt, Indonesia, and India [3]. Recent investigations suggest a higher risk of infection in microcephaly during pregnancy, several neurological complications such as Guillain-Barré syndrome, meningoencephalitis, acute respiratory distress syndrome, hepatic dysfunction, hemorrhagic complications, multi-organ dysfunction syndrome, and death [2, 4, 5].

The single-stranded positive-sense RNA genome of ZIKV translates into a long polyprotein in infected cells cytoplasm. The ZIKV polyprotein consists of three structural proteins [precursor membrane (prM) protein, envelope (E) protein, and capsid (C) protein] form the virus particle and seven non-structural proteins (NS1, NS2A, NS2B, NS3, NS4A, NS4B, and NS5) perform essential functions in polyprotein

processing, genome replication, and manipulation of host responses for viral advantage [6]. As an essential and imperative component of viral replication and forming membrane-bound complexes with other viral proteins, the NS3-Hel protein can be a most attractive antiviral target [7]. The multifunctional protein NS3 helicase possesses 5'-terminal RNA triphosphatase and nucleotide 5'-triphosphatase activities [8]. Fang et al. reported three crystal structures of ZIKV NS3 helicase comprising one in apo form and two in complex with ADP and  $Mn^{2+}$  [9]. The NS3-Hel comprises three domains with equal sizes, and apparent clefts locate between the adjacent domains (Fig. 1). The mechanism of flavivirus ATP hydrolysis in DENV NS3 helicase is illustrated in four states. The first state denotes the substrate complex using ATP analog, second state mimics the catalytic transition state using ADP, third state represents a form of both ADP and phosphate bound complex and fourth state represents a ADP bound product complex [10]. In the ATP bound substrate complex and ADP bound product complex of ZIKV NS3 and DENV NS3, the reactant water play essential role by forming hydrogen bonds with two conserved residues [9]. Domain 1 at residues 182–327 and domain 2 at residues 328–480 comprises the tandem  $\alpha/\beta$  RecA-like folds

**Fig. 1** The three domains of NS3-Hel protein binding pocket used for virtual screening



characteristic of SF1 and SF2 helicases [11]. Domain 1 is associated with the classical motifs I/P-loop (or Walker A), Ia, II (or Walker B), and III, whereas the motifs IV, IVa, V, and VI are involved in domain 2. These helicase motifs are typically associated with ATP binding and/or hydrolysis (motifs I, II, and VI), inter-domain communication, and RNA binding (motifs Ia, IV, and V) and line a cleft at the interface of domains 1 and 2 [12]. The C-terminus of NS3-Hel contains an NTP-dependent RNA helicase domain, and it is mainly responsible for the hydrolysis of NTPs and the unwinding of the RNA [13, 14]. Thus, NS3-Hel becomes a promising target for antiviral drug development programs.

Yuan et al. validated the ZIKV NS2B-NS3 protease inhibitor activity in novobiocin and lopinavir-ritonavir [15]. There are various repurposed drugs like chloroquine, emricasan, niclosamide, mycophenolic acid, mefloquine, bortezomib, suramin, sofosbuvir, nitazoxanide, and nitazoxanide, which inhibit the ZIKV replication but the molecular mechanism of inhibition is still unknown [16, 17]. The compounds CHEMBL619 and ZINC720 reported as hits for NTPase site of NS3 helicase protein [18].

To our knowledge, no potential and safe antiviral drugs or vaccines are available for the ZIKV. Therefore, a vaccine against the virus is urgently needed, and development is probably some years away [19]. Hence, alternative treatment options

are extremely required, both for prophylaxis of the infection to prevent and post-infection therapy. Molecular modeling and computational approaches are precious tools in developing potential inhibitors of ZIKV [20]. The structure-based drug design (SBDD) approach identifies leads to a target protein [21]. SBDD explores new insights on the nature of the active site and the ligand–protein interactions. This approach reduces the time and cost.

In this research investigation, we identified top inhibitors against ZIKV through various computational methods. In this study, we performed virtual screening to screen possible ZIKV inhibitors from the ZINC compound database. To evaluate drug-likeness, we completed the pharmacokinetics and toxicity parameters calculations of selected inhibitors. We also executed density functional theory calculations for top-scored compounds. We hope the results obtained from this research investigation would help search for novel potential inhibitors against ZIKV by identifying pharmacophoric and structural features involved in the binding process.

## Materials and methods

### Protein preparation

The three-dimensional crystal structure of Zika virus NS3 helicase at 1.8 Å resolutions with PDB-ID: 5JMT was retrieved from the Protein Data Bank (<http://www.rcsb.org/pdb>) [22, 23]. This resolution of the protein suggests its good quality as a resolution of 2.0 Å is the recommended maximum for the best structural protein for molecular modeling [24]. Restrained minimization was done through the OPLS-2005 force field and 0.3 Å as an RMSD constraint after optimizing hydrogen bonds.

### Active site identification

The catalytic site of the Zika virus NS3 helicase was identified using the SiteMap tool of Maestro. It recognizes potential active pocket by joining together “sitepoints” that most probably subsidize to tie protein–protein or protein–ligand binding [25, 26].

### Receptor grid generation

After preparing the protein and identifying the catalytic binding site, the receptor grid was generated for the protein by the Grid Generation panel of the Glide module. The receptor grid was generated to establish the active site of NS3 helicase protein prior to docking at the centroid of the predicted active sites. This technique generates two cubical boxes having a common centroid to organize the calculations: a larger enclosing and a smaller binding box [27].

### Ligand preparation and virtual screening

Virtual screening is a computational approach used in the drug discovery process to get small drug-like molecules that are most likely to bind the receptor or target molecule [28]. In this research work, the selected dataset consists of 0.5 million compound libraries of the ZINC database in SDF format [29]. The complete virtual screening was performed against the above-said databases by the Glide tool of Maestro. In this study, all selected dataset was screened for High throughput virtual screening (HTVS), Standard precision (SP) docking, and Extra precision (XP) docking [30]. Based on their Glide Gscore, drug likeness properties, the top five scoring compounds were selected for further investigation.

### Binding energy calculation

The molecular mechanics-generalized born surface area (MM-GBSA) method quantitatively measures the binding strength between the receptor and ligands [31]. Prime MM-GBSA panel of Maestro calculates the ligand binding as well as ligand strain energies of ligand–protein complexes. For this calculation, the top-scored ligand–protein complexes were selected with default parameters.

### Molecular dynamics simulations

MD simulation study was done through the Desmond tool of Maestro for protein–ligand complexes [32]. The top five compounds were considered for MD simulations based on their binding interactions (Glide Gscore), binding energy, pharmacokinetic, and toxicity parameters. The selected protein–ligand complex was pre-processed to refine side chains, add missing atoms, and minimize strain before MD simulation through the protein preparation wizard. The prepared complex was imported into the solvation tab of system builder panel. In this panel, a solvated model generates by selecting POPC (300 K) as a membrane model, SPC as a solvent model with an orthorhombic box shape. In the ions tab, the system neutralized by adding the required number of ions and 0.15 M as the salt concentration of Na<sup>+</sup> and Cl<sup>−</sup> ions to simulate the physiological conditions. All periodic boundary conditions were employed. All bad contacts were removed by energy minimization with the help of the hybrid method steepest decent and the limited-memory Broyden–Fletcher–Goldfarb–Shanno (LBFGS) algorithms [33]. Further, a minimized solvated model was imported into the molecular dynamics tab as “*out.cms*” file and simulation was carried out for 100 ns by keeping a 4.8 ps trajectory recording. The force field OPLS\_2005 was selected simulation calculations. The model was relaxed before the production system run because it makes a series of predefined minimizations and MD executions.

### Pharmacokinetic and toxicity parameters calculations

QikProp tool is used for calculation of pharmacokinetic properties of ligands as molecular weight (MW), molecular volume, hydrophobicity, hydrophilicity, polar surface area (PSA), number of the rotatable bond, donor and acceptor hydrogen bonds, etc. [34]. PSA is a very useful parameter for the prediction of drug transport properties. QPlogPo/w is the octanol/water partition coefficient which evaluates the lipophilicity of the compounds. QPlogS and QPlogBB predict the aqueous solubility and brain/blood partition coefficient of compounds, respectively. OSIRIS property explorer was used for the toxicity prediction of inhibitors of NS3 protein.

## Prediction of bioavailability and synthetic feasibility

In silico bioavailability and synthetic feasibility of the top-scored compounds were evaluated through the Swiss ADME tool. Consideration of synthetic practicability produces a number between 1- for simply synthesized compounds and 10- for compounds that are challenging to synthesize [35].

## Density functional theory calculations

Single point energy calculations using density functional theory were performed using Jaguar to explain ligand-bound protein at an electronic level. The chemical structures of ZINC01033978 and ZINC00114948 were optimized using hybrid functional B3LYP parameters with 6-31G\*\* basis set. Various properties such as electrostatic potential, average local ionization energy, gas-phase energy, canonical orbital, etc. were evaluated.

## Results and discussion

### Identification of active sites

For generating the active catalytic site, a comprehensive search was done by SiteMap for searching hydrogen-bonded, hydrophobic, and van der Waals regions in protein pockets. It results in five possible binding sites depicted in Table 1.

Based on exposure, enclosure, and covered by other features, scoring was done. The druggability of each binding

site had given in terms of the sitescore. In all possible binding sites, site\_1 has a maximum of 1.081 sitescore along with 1346.618 Å as volume. The sitescore of other site\_2, site\_3, site\_4, and site\_5 was 1.046, 0.830, 0.940, and 0.756. Due to excellent don/acc, volume, and Dscore value, site\_1 can mechanistically justify the binding pattern and answer for the protein–ligand interactions. Hence, site\_1 was considered an appropriate binding site to perform virtual screening based on sitescore and other structural features. The active site was made up of 42 amino acid residues, namely Pro292, Pro542, Val366, Ser601, Asp602, Asp540, Lys389, Val543, Glu489, Arg388, Leu442, Ser365, Pro364, Val363, Thr409, Cys429, Asp410, Leu430, Lys389, Arg598, Hid486, Arg617, Ser608, Phe609, Val599, Ala605, Leu541, Lys431, Pro432, Ser293, Ala264, Asp291, Thr290, Glu489, Met536, Leu493, Thr267, Phe289, Glu392, Met414, Gly539, and Hid484. The binding pocket of site\_1 diagram has given in supplementary data (Fig. S1).

### Virtual screening and binding interaction analysis of complexes

A dataset of small molecules of the ZINC database was used for the virtual screening of NS3 helicase protein (5JMT). Active sites with the best site scores (top-ranked potential receptor binding cavity) had been taken as a prerequisite for receptor grid generation. The executed virtual screening approach was using the hierarchical model of elimination technique, i.e. HTVS followed by SP and further the XP docking. The number of compounds employed for HTVS, SP and XP docking were 50,000, 5000 and 500, respectively. After the hierarchical model of screening, the top five inhibitors were considered for further studies. The GlideGscore and Prime MM-GBSA binding energy parameters score of all top-scored inhibitors is shown in Table 2.

The GlideGscore of ZINC01033978 was  $-7.55$  kcal/mol with two hydrogen bonds with the sidechain Ser601 and Asp602 amino acid residues (Table 3). This suggests that ZINC01033978 possesses greater affinity for NS3 helicase protein. A hydrophobic interaction was also observed between NS3 helicase protein and ZINC01033978 by Pro292, Val543, Pro542, Leu442, Val366, Pro364, Val363,

**Table 1** Structural features of the active sites predicted by SiteMap

Sitemap_site	Site_1	Site_2	Site_3	Site_4	Site_5
SiteScore	1.081	1.046	0.830	0.940	0.756
Dscore	1.107	0.971	0.825	0.866	0.722
Volume	1346.618	292.922	197.225	238.042	89.866
Exposure	0.453	0.531	0.653	0.642	0.604
Enclosure	0.791	0.767	0.620	0.659	0.632
Contact	1.027	0.980	0.888	0.880	0.882
Don/acc	0.902	0.513	1.440	1.301	0.289

**Table 2** Results of MMGBSA binding energies and docking score of top five inhibitors

Ligand No.	Glide Gscore	MMGBSA $\Delta G$ bind	MMGBSA $\Delta G$ bind coulomb	MMGBSA $\Delta G$ bind lipo	MMGBSA $\Delta G$ bind hbond	MMGBSA $\Delta G$ bind vdW
ZINC01033978	$-7.55$	$-62.709$	3.419	$-30.956$	$-1.235$	$-43.541$
ZINC00114948	$-7.42$	$-54.351$	$-25.893$	$-18.442$	$-1.864$	$-31.019$
ZINC01047185	$-7.41$	$-64.376$	$-28.789$	$-26.087$	$-1.707$	$-36.336$
ZINC12340356	$-7.33$	$-58.802$	$-28.955$	$-39.112$	$-5.041$	$-58.223$
ZINC01034603	$-7.30$	$-59.454$	$-22.089$	$-28.820$	$-3.135$	$-41.066$

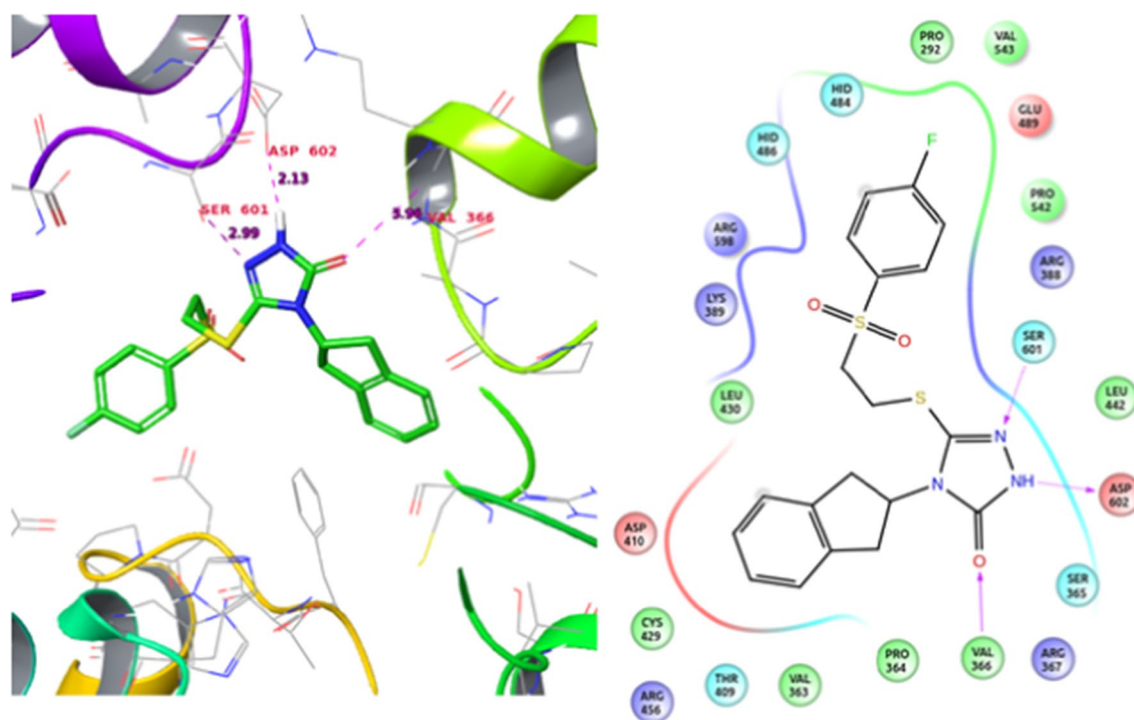
**Table 3** Top five screened inhibitors with their number of interacting hydrogen bonds, interacting residues, and other observed interactions

Ligand No.	No. of hydrogen bond		H-bond interaction		Other interactions
	Backbone	Sidechain	Backbone	Sidechain	
ZINC01033978	1	2	Val366	Ser601, Asp602	–
ZINC00114948	1	2	Asp540	Asp540, Lys389	–
ZINC01047185	1	2	Asp540	Asp540, Lys389	–
ZINC12340356	–	5	–	Ser293, Asp291, Arg598, Hid486, Arg388	$\Pi$ - $\Pi$ stacking, $\Pi$ -cation
ZINC01034603	1	4	Val543	Lys389, Arg598, Asp291	$\Pi$ - $\Pi$ stacking

Cys429, and Leu430 amino acid residues (Fig. 2). Similar to ZINC01033978, the ZINC00114948 compound interacts by hydrogen bonding with Asp540 and Lys389, which belongs to an essential cleft for viral replication (Fig. 3) [13].

ZINC01033978 is a triazole derivative characterized by an indane ring with a ketone group, and a fluorophenyl substituted group at positions 3 and 5. The two nitrogen of triazole ring involved in hydrogen bond interaction with Ser601 and Asp602 residues. These amino acid residues interact with the RNA motifs of NS3 protein [12]. Triazole nucleus play significant role in medicinal chemistry due to its capability of forming a hydrogen bond, which improves their solubility and ability to favorable interact with bimolecular targets. The 1,2,3-triazoles are highly stable to metabolic degradation as compared to other heterocyclic compounds because they have three adjacent nitrogen atoms [36, 37].

Compound ZINC01047185 interacts with sidechain residues Asp540 and Lys389 and backbone residue Asp540 to make hydrogen bonds (Supplementary Fig. S2). The residues Leu541, Pro542, Val599, Phe609, Ala605, Val366, Leu442, Leu430, and Pro432 show hydrophobic interactions with compound ZINC01047185. The other compound, ZINC12340356, forms five hydrogen bonds with the sidechain residues Ser293, Asp291, Arg598, Hid486, and Arg388 (Supplementary Fig. S3). The  $\pi$ - $\pi$  stacking has also been observed between NS3 helicase protein and benzene ring of ZINC12340356 by Arg598 residue. Same as the compound, ZINC01034603 interacts by hydrogen bonding with Asp291, Arg598, and Lys389, and Val543 amino acid residues. In addition, the pyrazole ring was involved in  $\pi$ - $\pi$  stacking interaction with NS3 helicase protein by Arg598 residue (Supplementary Fig. S4). Epigallocatechin-3-Gallate binds with RNA binding cavity by forming hydrogen bond

**Fig. 2** NS3 helicase protein and ZINC01033978 binding interaction diagram

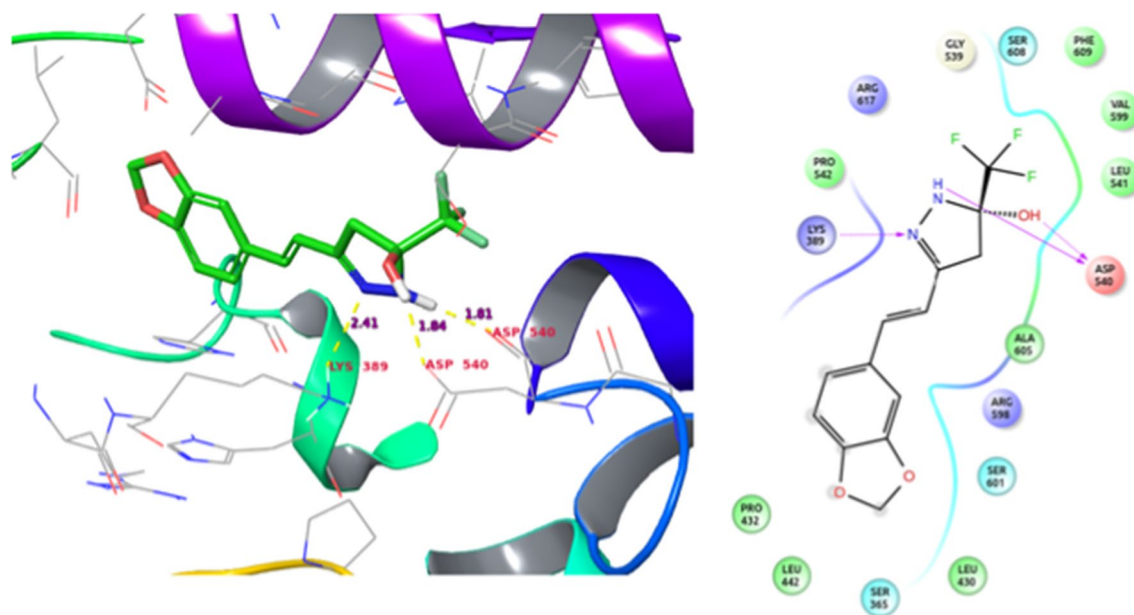


**Fig. 3** NS3 helicase protein and ZINC00114948 binding interaction diagram

**Table 4** Observed RMSD and RMSF values of top five screened inhibitors

Ligand–protein complex	RMSD (Å)	RMSF (Å)
ZINC01033978	2.05	1.75
ZINC00114948	1.70	1.50
ZINC01047185	1.65	1.50
ZINC12340356	1.80	1.50
ZINC01034603	2.50	1.25

with Leu430 [38]. This indicates similar binding of screened compounds.

### Molecular dynamics simulations analysis

MD simulation enables the atomic-level characterization of numerous biomolecular processes, such as analyzing the stability of protein–ligand interactions associated with activation and deactivation of various molecular pathways. The stability analysis of all top-scored inhibitors was carried out by the Desmond tool.

The simulation study of complexes was performed for 10,000 ps after the system minimization with 2000 iterations. The observed root mean square deviation (RMSD) and root mean square fluctuation (RMSF) is shown in Table 4.

For the ZINC01033978 compound, the RMSD indicates good stability in the NS3 Hel binding site, suggesting this molecule may represent a potential NS3 Hel inhibitor. The

amino acid residues Val366, Ser601, Asp602, and Ser365 were involved in hydrogen bond interactions, and Pro292, Lys389, Met414, Cys429, Leu430, Leu442, His486, Pro542 residues form the hydrophobic interactions with ZINC01033978 (Fig. 4). The hydrophobic interactions involved a hydrophobic amino acid and an aromatic or aliphatic group on the ZINC01033978. The residue Glu392 was found to be involved in polar or ionic interactions between two oppositely charged atoms within 3.7 Å.

Similarly, the compound ZINC00114948 was found to be able to form hydrogen bonds with Asp540, Lys389 and Ser608 (Fig. 5). Therefore, the residue Asp540 plays an essential role in the binding mechanism due to hydrogen bonds forming with sidechain and backbone residue. Moreover, ZINC00114948 interacts with Leu442, Pro432 and Ala605 residues through hydrophobic interactions suggesting this compound is also an attractive lead molecule towards ZIKV NS3 Hel inhibitors. These results are consistent with molecular docking studies. Therefore, docking results are found validated through MD simulation calculations.

As shown by MD simulation of compounds ZINC01047185, ZINC12340356 and ZINC01034603, the system was found to be perfectly equilibrated and acceptable for small, globular proteins (Supplementary Figs. S5, S6, S7). The hydrophobic interactions enhance the binding affinity; hence, the residue Pro542, Cys429, Pro432, Leu442 and Ala605 consist of the NS3-Hel binding pockets hydrophobic region.

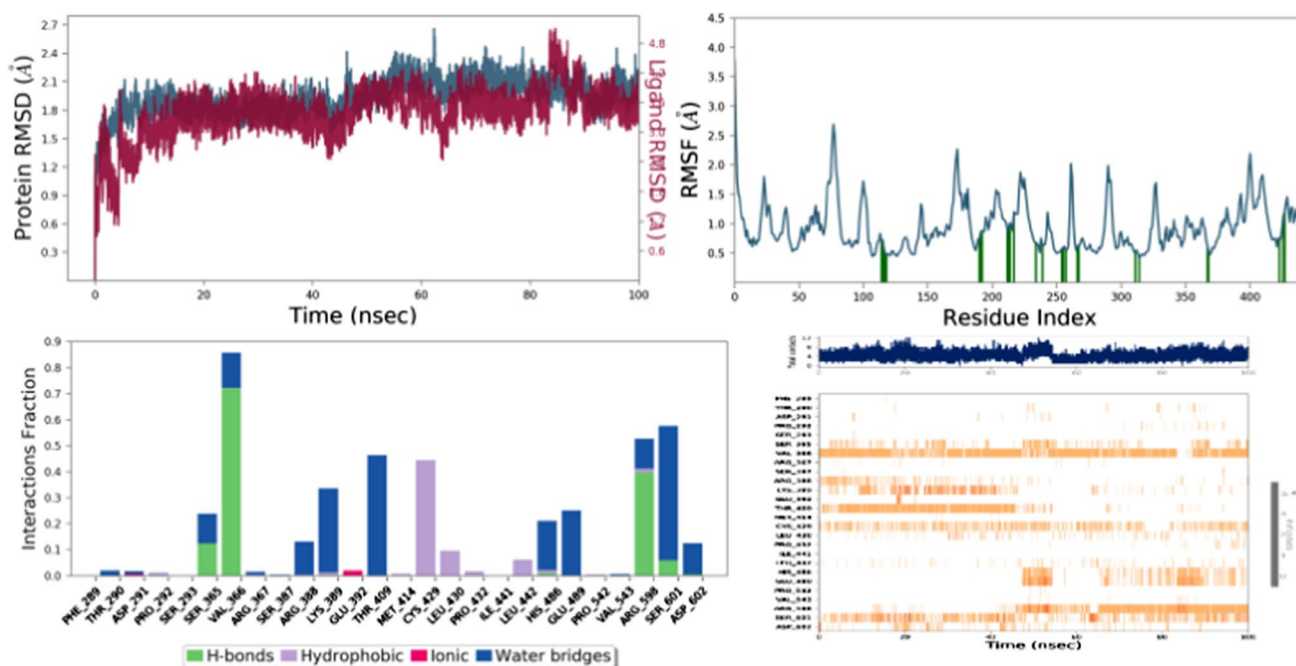


Fig. 4 The protein RMSD, RMSF, and protein–ligand contacts diagram of complex 5JMT with ZINC01033978

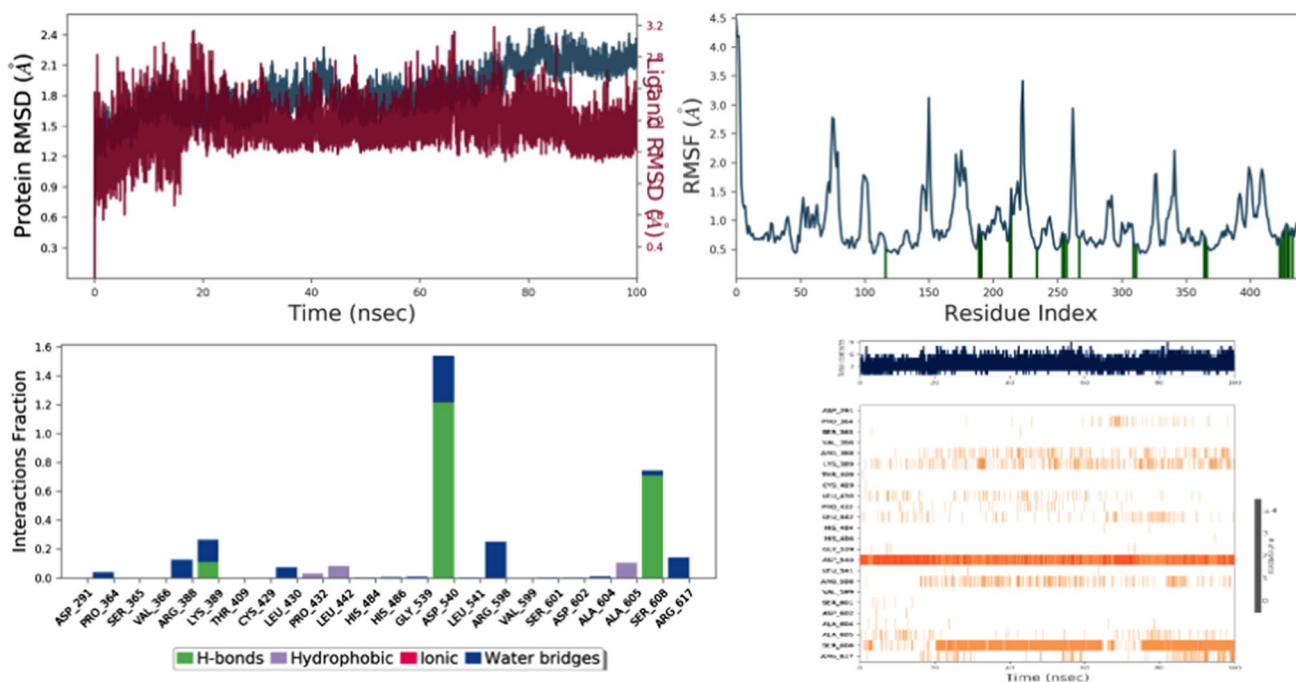


Fig. 5 The protein RMSD, RMSF, and protein–ligand contacts diagram of complex 5JMT with ZINC00114948

### Pharmacokinetic, toxicity parameters and bioavailability analysis

Lipinski's rule of five was one factor used to assure the drug-like (oral) pharmacokinetics profile of the ligands.

The various physicochemical and significant therapeutic descriptors were calculated through the Qikprop tool and depicted in Tables 5 and 6, respectively. All top-scored inhibitors show no violation of Lipinski's rule of five and



have been found in an acceptable range of all pharmacokinetic parameters.

The toxicity parameters of all top-scored inhibitors were evaluated through OSIRIS property explorer. None of the toxic profiles has been found in most selected inhibitors except ZINC00114948 and ZINC01047185, which shows a high reproductive effect. All evaluated parameters are listed in Table 7.

The boiled egg diagram (Fig. 6) expresses brain penetration and human intestinal absorption (HIA). The yellow region (yolk) and the white region (albumin) denote the area where there is a high chance of brain penetration and human intestinal absorption, respectively. Only inhibitor ZINC00114948 falls within the yellow region to imply

a high probability of brain penetration and being absorbed by the gastrointestinal tract. In contrast, compounds ZINC01033978, ZINC01047185, ZINC12340356, and ZINC01034603 fall in the white region signify their high chances of being absorbed by the gastrointestinal tract only. We also generated the bioavailability radar chart through the SwissADME tool, which gives a quick look at the drug-likeness of top scored inhibitors [38, 39]. The predicted bioavailability score is shown in Table 8.

In bioavailability radar charts, the pink area represents the most favorable area for each property. FLEX, LIPO, SIZE, and POLAR all refer to rotatable bonds, logP, molecular weight, and polar surface area, respectively. The inhibitor ZINC01033978 was the best of the other selected inhibitors

**Table 5** Principle pharmacokinetic parameters of top five screened inhibitors

Ligand No.	MW	Dipole	DonorHB	AcceptHB	Volume	Rotor	PSA	Rule of Five
ZINC01033978	419.488	5.783	1.00	7.00	1180.429	5	93.885	0
ZINC00114948	300.237	2.414	2.00	3.500	825.108	4	68.725	0
ZINC01047185	351.346	3.399	3.00	2.500	954.981	1	62.124	0
ZINC12340356	460.485	5.692	2.50	7.500	1432.404	10	163.537	0
ZINC01034603	384.821	7.955	1.00	4.00	1195.333	4	94.892	0
Range <sup>a</sup>	130.0–725.0	1.0–12.5	1.0–6.0	2.0–20.0	500.0–2000.0	0–15	7.0–200	Max 4

<sup>a</sup>Range: for 95% oral drugs

**Table 6** Therapeutic significant parameters of top five screened inhibitors

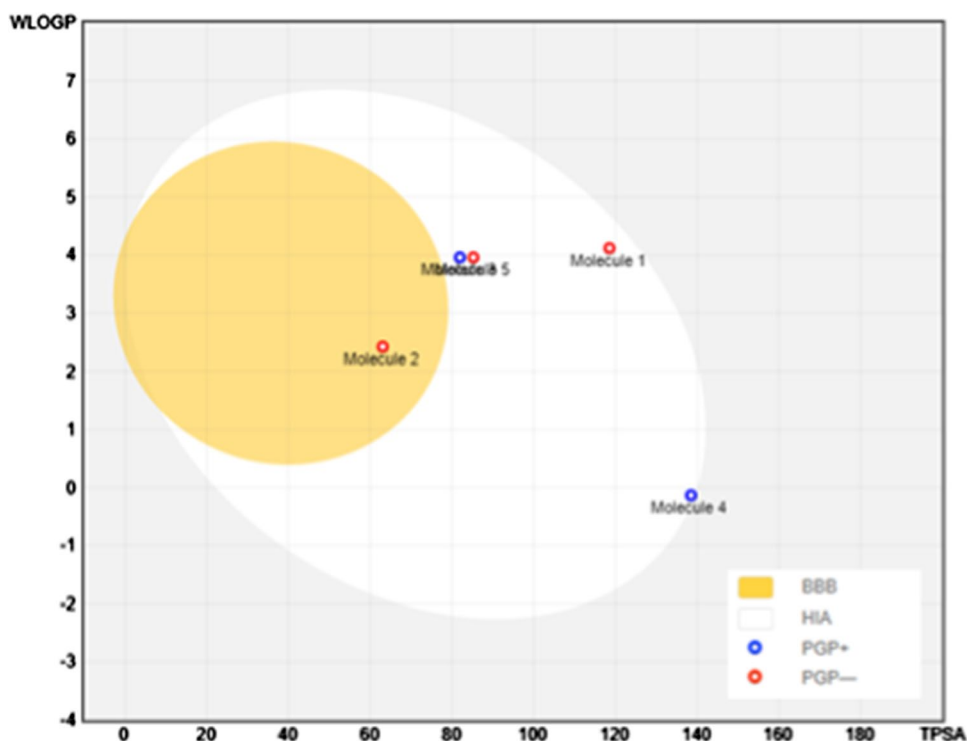
Ligand No.	CNS	QPlogPo/w	QPlogS	QPlogBB	QPPMDCK	Metab	QPlogKhsa	Percent HOA
ZINC01033978	-2	3.366	-5.141	-1.029	425.695	2	0.238	92.96
ZINC00114948	0	2.849	-3.638	-0.147	3188.215	2	-0.021	100.00
ZINC01047185	0	4.066	-5.352	0.085	4989.126	7	0.467	100.00
ZINC12340356	-2	4.857	-6.229	-2.690	1.822	4	0.207	65.31
ZINC01034603	0	4.512	-6.229	-0.566	1390.008	1	0.593	100.00
Range <sup>a</sup>	-2 to +2	-2 to 6.5	-6.5 to 0.5	-3.0 to 1.2	<25 poor >500 great	1 to 8	-1.5 to 1.5	>80% high <25% poor

<sup>a</sup>Range: for 95% oral drugs

**Table 7** Toxicity parameters of the top five screened inhibitors

Toxicity parameters	ZINC 01033978	ZINC 00114948	ZINC 01047185	ZINC 12340356	ZINC 01034603
Mutagenic	No	No	No	No	No
Tumorigenic	No	No	No	No	No
Irritant	No	No	No	No	No
Reproductive effect	No	Highly	Highly	No	No
cLogP	3.01	2.7	4.16	2.4	3.25
Solubility	-5.74	-4.4	-5.82	-4.2	-5.08
TPSA	112.5	63.08	81.95	132.8	85.25
Druglikeness	-5.21	-7.93	-6.46	-16.8	1.52
Drug score	0.27	0.23	0.15	0.33	0.56

**Fig. 6** The EGG-BOILED model for top scored compound (Fig. S8).



as it falls within the acceptable range for all parameters. The bioavailability radar charts are shown in supplementary data (Fig. S8).

### Estimation of synthetic feasibility

According to Ertl and Schuffenhauer, “the synthetic accessibility score is in the range of 1 for simply synthesizable and 10 for challenging to synthesize” [40]. All top-scored inhibitors show a synthetic feasibility score of around 3.0, indicating that all are easily synthesizable (Table 8). Furthermore, we forward to plan future synthesis with the best plausible route.

### DFT calculations

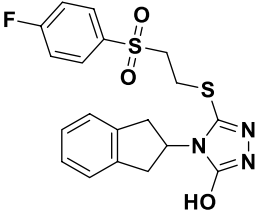
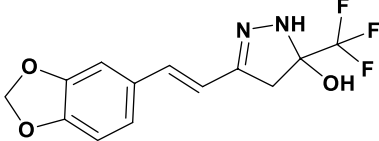
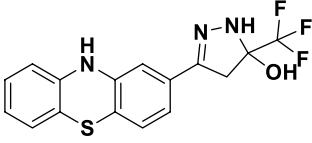
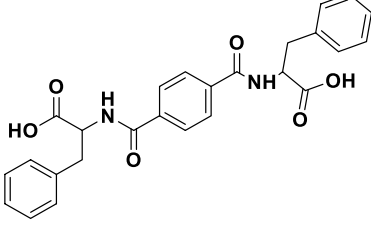
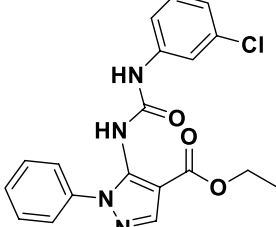
Two top-scored compounds were chosen for energy calculations. The electronic interactions of the compounds play a vital role in biological effects. Therefore, the position of LUMO–HOMO is responsible for the electron transfer in reaction. Properties like vibrational frequencies, HOMO energy, LUMO energy, ESP, and interaction strength were calculated using Jaguar (Table 9) (Figs. 7, 8).

### Conclusion

In conclusion, a structure-based virtual screening and molecular dynamics simulation study were carried out to discover novel, potential NS3 helicase protein inhibitors.

Due to the most imperative viral replication component, targeting NS3-Hel protein is quite an attractive approach to treat ZIKV. The active site of the NS3 helicase protein consists of 42 amino acid residues. The top five inhibitors were selected based on GlideGscore. The highest scoring inhibitor ZINC01033978 (7.55 kcal/mol) exhibits three hydrogen bonds with amino acid residues Ser601, Val366, and Asp602. The docking analysis suggests that the NS3-Hel protein binding pocket is consists of hydrophobic (Phe609, Val599, Leu541, Ala605, Leu430, Leu442, Pro432, Pro292, Val543, Pro542, and Pro364) part, H-bond (Asp540, Lys289, Ser601, Asp602, Val366, Arg598, Asp291, Lys389, Ser293, and Hid486) part and  $\pi$ - $\pi$  stacking residues (Arg598). The RMSD of NS3-Hel protein with inhibitors was found in the range of 1.65 to 2.50 Å, indicating the simulation has equilibrated, and changes are perfectly acceptable for small, globular proteins. Hence, both docking and molecular dynamics simulation investigations revealed that the top-scored inhibitors have a strong binding affinity towards the NS3 helicase protein. Thus, screened compounds as potential inhibitors against the NS3-Hel ZIKV. The pharmacokinetic analysis revealed that top-scored inhibitors have no violation of Lipinski’s rule of five, confirms drug-likeness ability. The toxicity parameters are also found in the acceptable range except for the reproductive effect. All top-scored inhibitors are easily synthesizable, having the least synthetic accessibility score. Experimentally, the need to validate the molecular modeling results reported here with in vitro

**Table 8** Synthetic accessibility and bioavailability score of top five screened inhibitors

Ligand No.	Hit structures	Bioavailability score	Synthetic feasibility score
ZINC01033978		0.55	3.68
ZINC00114948		0.55	3.69
ZINC01047185		0.55	3.64
ZINC12340356		0.56	3.16
ZINC01034603		0.55	3.01

**Table 9** Summary of calculated electronic properties of hit molecules

Electronic properties	ZINC01033978	ZINC00114948
No. of canonical orbitals	516	369
Gas phase energy	- 2020.938130	- 1136.642406
HOMO	- 0.21609	- 0.19502
LUMO	- 0.04831	- 0.05568
Electrostatic potential mean (kcal/mol)	1.16	0.76
Average local ionization energy mean (kcal/mol)	267.15	279.53

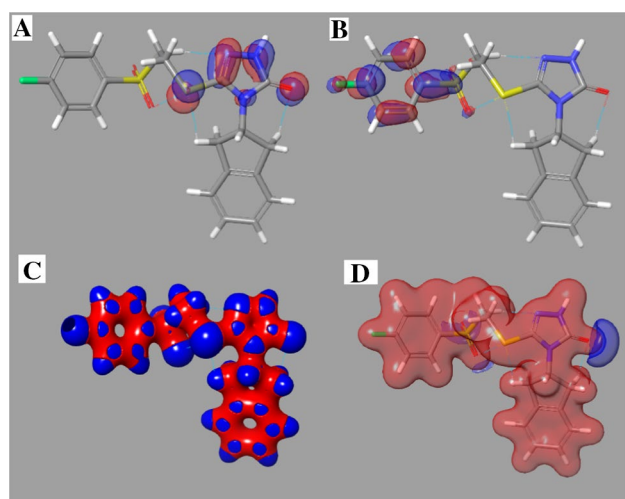


**Fig. 7** DFT results for ZINC01033978: **A** HOMO map **B** LUMO map **C** Interaction strength map **D** Electrostatic potential map

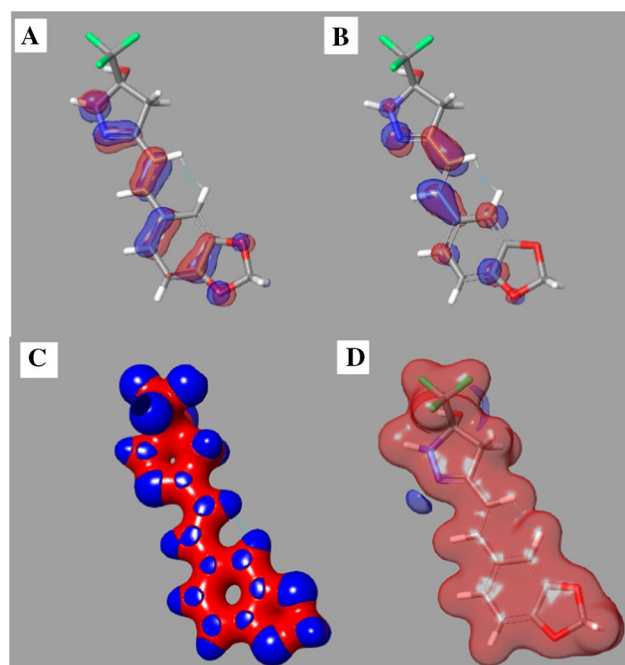


**Fig. 8** DFT results for ZINC00114948: **A** HOMO map **B** LUMO map **C** Interaction strength map **D** Electrostatic potential map

and/or in vivo inhibition evaluation is acknowledged. Still, due to lack of funding, work is limited. Therefore, investigated inhibitors could be provided the lead to the targeting NS3-Hel protein for the ZIKV treatment.

**Supplementary Information** The online version contains supplementary material available at <https://doi.org/10.1007/s11030-022-10522-5>.

## Declarations

**Conflicts of interest** No competing interests exist.

## References

- Marin MS, Zanotto PDA, Gritsun TS, Gould EA (1995) Phylogeny of TYU, SRE, and CFA virus: different evolutionary rates in the genus flavivirus. *Virology* 206(2):1133–1139. <https://doi.org/10.1006/viro.1995.1038>
- Paixão ES, Barreto F, da Glória Teixeira M, da Conceição N, Costa M, Rodrigues LC (2016) History, epidemiology, and clinical manifestations of Zika: a systematic review. *Am J Public Health* 106(4):606–612. <https://doi.org/10.2105/ajph.2016.303112>
- Campos GS, Bandeira AC, Sardi SI (2015) Zika virus outbreak, bahia, brazil. *Emerg Infect Dis* 21(10):1885. <https://doi.org/10.3201/eid2110.150847>
- Arzuza-Ortega L, Polo A, Pérez-Tatis G, López-García H, Parra E, Pardo-Herrera LC, Rodríguez-Morales AJ (2016) Fatal sickle cell disease and Zika virus infection in girl from Colombia. *Emerg Infect Dis* 22(5):925. <https://doi.org/10.3201/eid2205.151934>
- Azevedo RS, Araujo MT, Martins Filho AJ, Oliveira CS, Nunes BT, Cruz AC, Vasconcelos PF (2016) Zika virus epidemic in Brazil. I. Fatal disease in adults: clinical and laboratorial aspects. *J Clin Virol* 85:56–64. <https://doi.org/10.1016/j.jcv.2016.10.024>
- Fernandez-Garcia MD, Mazzon M, Jacobs M, Amara A (2009) Pathogenesis of flavivirus infections: using and abusing the host cell. *Cell Host Microbe* 5(4):318–328. <https://doi.org/10.1016/j.chom.2009.04.001>
- Salonen ANNE, Ahola TERO, Kääriäinen LEEVI (2004) Viral RNA replication in association with cellular membranes. *Membr Traffick Viral Replication*. [https://doi.org/10.1007/3-540-26764-6\\_5](https://doi.org/10.1007/3-540-26764-6_5)
- Yamashita T, Unno H, Mori Y, Tani H, Moriishi K, Takamizawa A, Matsuura Y (2008) Crystal structure of the catalytic domain of Japanese encephalitis virus NS3 helicase/nucleoside triphosphatase at a resolution of 1.8 Å. *Virology* 373(2):426–436. <https://doi.org/10.1016/j.virol.2007.12.018>
- Fang J, Jing X, Lu G, Xu Y, Gong P (2019) Crystallographic snapshots of the Zika Virus NS3 helicase help visualize the reactant water replenishment. *ACS Infectious Dis* 5(2):177–183. <https://doi.org/10.1021/acsinfecdis.8b00214>
- Luo D, Xu T, Watson RP, Scherer-Becker D, Sampath A, Jahnke W, Lescar J (2008) Insights into RNA unwinding and ATP hydrolysis by the flavivirus NS3 protein. *EMBO J* 27(23):3209–3219. <https://doi.org/10.1038/emboj.2008.232>
- Singleton MR, Dillingham MS, Wigley DB (2007) Structure and mechanism of helicases and nucleic acid translocases. *Annu Rev Biochem* 76:23–50. <https://doi.org/10.1146/annurev.biochem.76.052305.115300>
- Jain R, Coloma J, García-Sastre A, Aggarwal AK (2016) Structure of the NS3 helicase from Zika virus. *Nat Struct Mol Biol* 23(8):752–754. <https://doi.org/10.1038/nsmb.3258>
- Matusan AE, Pryor MJ, Davidson AD, Wright PJ (2001) Mutagenesis of the Dengue virus type 2 NS3 protein within and outside helicase motifs: effects on enzyme activity and virus replication. *J Virol* 75(20):9633–9643. <https://doi.org/10.1128/jvi.75.20.9633-9643.2001>

14. Sampath A, Xu T, Chao A, Luo D, Lescar J, Vasudevan SG (2006) Structure-based mutational analysis of the NS3 helicase from dengue virus. *J Virol* 80(13):6686–6690. <https://doi.org/10.1128/jvi.02215-05>
15. Yuan S, Chan JFW, den-Haan H, Chik KKH, Zhang AJ, Chan CCS, Yuen KY (2017) Structure-based discovery of clinically approved drugs as Zika virus NS2B-NS3 protease inhibitors that potently inhibit Zika virus infection in vitro and in vivo. *Antivir Res* 145:33–43. <https://doi.org/10.1016/j.antiviral.2017.07.007>
16. Devillers J (2018) Repurposing drugs for use against Zika virus infection. *SAR QSAR Environ Res* 29(2):103–115. <https://doi.org/10.1080/1062936x.2017.1411642>
17. Xu M, Lee EM, Wen Z, Cheng Y, Huang WK, Qian X, Tang H (2016) Identification of small-molecule inhibitors of Zika virus infection and induced neural cell death via a drug repurposing screen. *Nat Med* 22(10):1101–1107. <https://doi.org/10.1038/nm.4184>
18. Kumar D, Aarthy M, Kumar P, Singh SK, Uversky VN, Giri R (2020) Targeting the NTPase site of Zika virus NS3 helicase for inhibitor discovery. *J Biomol Struct Dyn* 38(16):4827–4837. <https://doi.org/10.1080/07391102.2019.1689851>
19. Retalack H, Di Lullo E, Arias C, Knopp KA, Laurie MT, Sandoval-Espinosa C, DeRisi JL (2016) Zika virus cell tropism in the developing human brain and inhibition by azithromycin. *Proc Natl Acad Sci USA* 113(50):14408–14413. <https://doi.org/10.1073/pnas.1618029113>
20. Kumar N, Mishra SS, Sharma CS, Singh HP, Kalra S (2018) In silico binding mechanism prediction of benzimidazole based corticotropin releasing factor-1 receptor antagonists by quantitative structure activity relationship, molecular docking and pharmacokinetic parameters calculation. *J Biomol Struct Dyn* 36(7):1691–1712. <https://doi.org/10.1080/07391102.2017.1332688>
21. Azam MA, Jupudi S, Saha N, Paul RK (2019) Combining molecular docking and molecular dynamics studies for modelling *Staphylococcus aureus* MurD inhibitory activity. *SAR QSAR Environ Res* 30(1):1–20. <https://doi.org/10.1080/1062936x.2018.1539034>
22. Tian H, Ji X, Yang X, Xie W, Yang K, Chen C, Yang H (2016) The crystal structure of Zika virus helicase: basis for antiviral drug design. *Protein Cell* 7(6):450–454. <https://doi.org/10.1007/s13238-016-0275-4>
23. Berman HM, Battistuz T, Bhat TN, Bluhm WF, Bourne PE, Burkhardt K, Zarddecki C (2002) The protein data bank. *Acta Crystallogr D* 58(6):899–907. <https://doi.org/10.1107/s0907444902003451>
24. Hajduk PJ, Huth JR, Tse C (2005) Predicting protein druggability. *Drug Discov Today* 10(23–24):1675–1682. [https://doi.org/10.1016/s1359-6446\(05\)03624-x](https://doi.org/10.1016/s1359-6446(05)03624-x)
25. Halgren T (2007) New method for fast and accurate binding-site identification and analysis. *Chem Biol Drug Des* 69(2):146–148. <https://doi.org/10.1111/j.1747-0285.2007.00483.x>
26. Grinter SZ, Zou X (2014) Challenges, applications, and recent advances of protein-ligand docking in structure-based drug design. *Molecules* 19(7):10150–10176. <https://doi.org/10.3390/molecules190710150>
27. Athar M, Lone MY, Khedkar VM, Jha PC (2016) Pharmacophore model prediction, 3D-QSAR and molecular docking studies on vinyl sulfones targeting Nrf2-mediated gene transcription intended for anti-Parkinson drug design. *J Biomol Struct Dyn* 34(6):1282–1297. <https://doi.org/10.1080/07391102.2015.1077343>
28. Korkmaz S, Zararsiz G, Goksuluk D (2014) Drug/nondrug classification using support vector machines with various feature selection strategies. *Comput Methods Programs Biomed* 117(2):51–60. <https://doi.org/10.1016/j.cmpb.2014.08.009>
29. Rowley JD (1973) A new consistent chromosomal abnormality in chronic myelogenous leukaemia identified by quinacrine fluorescence and Giemsa staining. *Nature* 243(5405):290–293. <https://doi.org/10.1038/243290a0>
30. Kumar H, Raj U, Gupta S, Varadwaj PK (2016) In-silico identification of inhibitors against mutated BCR-ABL protein of chronic myeloid leukemia: a virtual screening and molecular dynamics simulation study. *J Biomol Struct Dyn* 34(10):2171–2183. <https://doi.org/10.1080/07391102.2015.1110046>
31. Genheden S, Kuhn O, Mikulskis P, Hoffmann D, Ryde U (2012) The normal-mode entropy in the MM/GBSA method: effect of system truncation, buffer region, and dielectric constant. *J Chem Inf Model* 52(8):2079–2088. <https://doi.org/10.1021/ci3001919>
32. Bowers KJ, Chow DE, Xu H, Dror RO, Eastwood MP, Gregersen BA, Shaw DE (2006) Scalable algorithms for molecular dynamics simulations on commodity clusters. In SC'06: Proceedings of the 2006 ACM/IEEE Conference on Supercomputing (pp. 43–43). IEEE. <https://doi.org/10.1145/1188455.1188544>
33. Guo Z, Mohanty U, Noehre J, Sawyer TK, Sherman W, Krilov G (2010) Probing the  $\alpha$ -helical structural stability of stapled p53 peptides: molecular dynamics simulations and analysis. *Chem Biol Drug Des* 75(4):348–359. <https://doi.org/10.1111/j.1747-0285.2010.00951.x>
34. Shekhar MS, Venkatachalam T, Sharma CS, Singh HP, Kalra S, Kumar N (2018) Computational investigation of binding mechanism of substituted pyrazinones targeting corticotropin releasing factor-1 receptor deliberated for anti-depressant drug design. *J Biomol Struct Dyn*. <https://doi.org/10.1080/07391102.2018.1513379>
35. Mishra SS, Ranjan S, Sharma CS, Singh HP, Kalra S, Kumar N (2021) Computational investigation of potential inhibitors of novel coronavirus 2019 through structure-based virtual screening, molecular dynamics and density functional theory studies. *J Biomol Struct Dyn* 39(12):4449–4461. <https://doi.org/10.1080/07391102.2020.1791957>
36. Chandrashekar M, Nayak VL, Ramakrishna S, Mallavadhani UV (2016) Novel triazole hybrids of myrrhanone C, a natural polypodane triterpene: synthesis, cytotoxic activity and cell based studies. *Eur J Med Chem* 114:293–307
37. Madasu C, Karri S, Sangaraju R, Sistla R, Uppuluri MV (2020) Synthesis and biological evaluation of some novel 1,2,3-triazole hybrids of myrrhanone B isolated from *Commiphora mukul* gum resin: identification of potent antiproliferative leads active against prostate cancer cells (PC-3). *Eur J Med Chem* 188:111974. <https://doi.org/10.1016/j.ejmech.2019.111974>
38. Daina A, Michielin O, Zoete V (2017) SwissADME: a free web tool to evaluate pharmacokinetics, drug-likeness and medicinal chemistry friendliness of small molecules. *Sci Rep* 7(1):1–13. <https://doi.org/10.1038/srep42717>
39. Kumar D, Sharma N, Aarthy M, Singh SK, Giri R (2020) Mechanistic insights into Zika virus NS3 helicase inhibition by Epigallocatechin-3-gallate. *ACS Omega* 5(19):11217–11226. <https://doi.org/10.1021/acsomega.0c01353>
40. Ertl P, Schuffenhauer A (2009) Estimation of synthetic accessibility score of drug-like molecules based on molecular complexity and fragment contributions. *J Cheminform* 1(1):1–11. <https://doi.org/10.1186/1758-2946-1-8>

**Publisher's Note** Springer Nature remains neutral with regard to jurisdictional claims in published maps and institutional affiliations.

Springer Nature or its licensor holds exclusive rights to this article under a publishing agreement with the author(s) or other rightsholder(s); author self-archiving of the accepted manuscript version of this article is solely governed by the terms of such publishing agreement and applicable law.